

PRIP-TR-3

Integration of SAR and DEM data - Geometrical Considerations

Walter G. Kropatsch

Abstract

General principles for integrating data from different sources are derived from the experience of registration of SAR images with DEM data. The integration in our case consists of establishing geometrical relations between the data sets that allow to accumulate information from both data sets for any given object point (e.g. elevation, slope, backscatter of ground cover, etc.).

Since the geometries of the two data are completely different they cannot be compared on a pixel by pixel basis. The presented approach detects instances of higher level features in both data sets independently and performs the matching at the high level. Besides the efficiency of this general strategy it further allows the integration of additional knowledge sources: world knowledge and sensor characteristics are also useful sources of information.

The SAR features layover and shadow can be detected easily in SAR images. An analytical method to find such regions also in a DEM needs in addition the parameters of the flight path of the SAR sensor and the range projection model. The generation of the SAR layover and shadow maps is summarized and new extensions to this method are proposed.

1 Introduction

Synthetic Apertur Radar (SAR) images differ strongly from conventional optical images by their image formation principle. Since SAR is an active sensor, image acquisition does not depend on local wheather conditions, which is a major advantage over all optical sensors especially in areas of the world that are often covered by clouds. Hence, many of the planned remote sensing systems include a SAR sensor. On the other side, SAR images are still very noisy data and are difficult to interpret by a photo-interpreter.

One of the reasons are the complex geometric distortions that are introduced by mapping the earth with a range projection. There exist several possibilities to remove these systematic distortions and to transform the SAR image into a map projection which should be easier to interpret. This process is called 'geocoding'. Several geocoding transformations are based on digital elevation models (DEM), especially in moutainous areas. Domik (1985) used image simulation; Raggam, Strobl, and Triebnig (1986) used squint angle condition and bundle adjustment; Meier and Nüesch (1986) used doppler information and target point velocity; Kwok, Curlander, and Pang (1987) used doppler information and a three pass resampling.

Most of the current approaches determine in a first step control points. A control point identifies the locations of one feature in reality in both data sets. It is represented by a pair of coordinates that is used to establish the geometrical correspondences between the two data sets. The set of all control points could be input to the geometric rectification procedure which combines interpolation and resampling or it could be simply used to localize a given object point in both data sets.

If both data sets show similar characteristics then similarity of image features can be used to find control points. But this is not possible if the data look completely different. In some cases one data set can be transformed such that the result shows optical resemblance with the other data set (at least locally). Then corresponding features can be detected by local similarity measurements (e.g. correlation). Most of the common methods compare pixel values of both images. Guindon (1987) and Sasse (1989) use automatic correlation to find the control points; Strobl (1986) uses manual matching for that purpose.

In the geocoding of SAR images, DEM data are often used to simulate the SAR geometry. But such geometric image transformations are computationally very expensive operations and have to be repeated not seldom to further adjust transformation parameters.

In Kropatsch and Strobl (1990) we have designed a different strategy to integrate SAR images and DEM data. The idea is based on the fact that real world objects are mapped differently in both data sets. Therefore we need also different operators to detect instances of the same object in the two data sets. Such feature detectors produce sets, F1 and F2, of image features with individual properties and with feature-to-feature relations in both data independently. Knowing the formation principles of the data sources, properties and relations of the features can be derived from properties and relations of the real world objects. Hence features from F1 and F2 can be matched via the corresponding objects in reality. This general approach has two main advantages:

1. Since image operators are derived from properties of real objects, the resulting features also relate to the semantics of these objects. Real world knowledge as a third information source can be efficiently applied for further processing.
2. The image-to-feature mapping reduces the data amount considerably, while, at the same time, the expressive power of the vocabulary to describe the image contents (e.g. the features) increases. Less data can be matched with less computation and more features can be differentiated by the greater vocabulary. Moreover, this generalization (or abstraction) process can be repeated.

2 SAR processing

Global characteristics of a SAR image include the parameters of the range projection, the resolution, and the flight path of the sensor. DEM data do not contain information about the type of the surface cover which is an important constituent of the SAR image. SAR images of mountainous areas often show characteristic features that do not severely depend on the backscattering of the surface cover: **layover** and **shadow**. Due to the multiplication of signals, layover regions appear brighter than the surrounding regions. Shadow regions, which appear as dark regions in the SAR image, are independent from the backscattering of the imaged terrain.

The flight path allows to distinguish between foreslopes and backslopes of the mountains. Foreslopes are oriented towards the sensor's path on the ground and are the (only) areas where layover can occur. Backslopes face the opposite direction and cannot be reached by the radar beam under certain imaging conditions (low sensor position or steep slope). Both types of features can be detected in a SAR image (Fig. 1) by a combination of noise elimination (i.e. filtering), thresholding, and connected component labeling (Plößnig, Billington, and Kropatsch, 1989; Plößnig, Kropatsch, and Strobl, 1989). The result is a set of layover and shadow regions in the SAR image (e.g. layover regions in Fig. 2).

3 DEM processing

Global parameters of a DEM are a reference coordinate system and the resolutions both in the ground plane ($\Delta x, \Delta y$) and in the elevation (Δz). Using the parameters of the SAR flight path, a sequence of operations is applied to the DEM data in order to detect layover and shadow regions also in the DEM geometry. The mathematical model (Kropatsch and Strobl, 1990) is based on differential analysis of the range and look angle functions derived from a continuous terrain. The discrete implementation includes local differentiation and a pointwise computation of decision functions. A search is necessary to complete the layover and shadow regions by their passive parts.

Figure 1: SAR-image of Iceland

Figure 2: Layover regions

3.1 Layover in the DEM

The characteristic radar measurements are **range** - the distance from the sensor to an object point - and **time** - the position of the sensor along its flight path where the data are collected. They define the two dimensional SAR image space.

Layover is called the radar mapping, where different object points having the same time and the same range are mapped into one image point, i.e. more than one points on the Earth's surface are mapped into one image point (many to one mapping). SAR mapping is mainly an integration of reflected signals having the same doppler frequency (azimuth or along track measurement) and the same distance (range or across track measurement).

In the object space the layover region splits into **active** and **passive** subregions. Active layover regions are the sources for layover (points that produce layover in the SAR image) whereas layover passives are only part of the layover because the active parts lay over them. The active layover region is embedded in two passive regions (called 'near passive' and 'far passive'). The calculation of the passive regions needs sequential search when no image simulation technique is used. In the image space there is no such distinction.

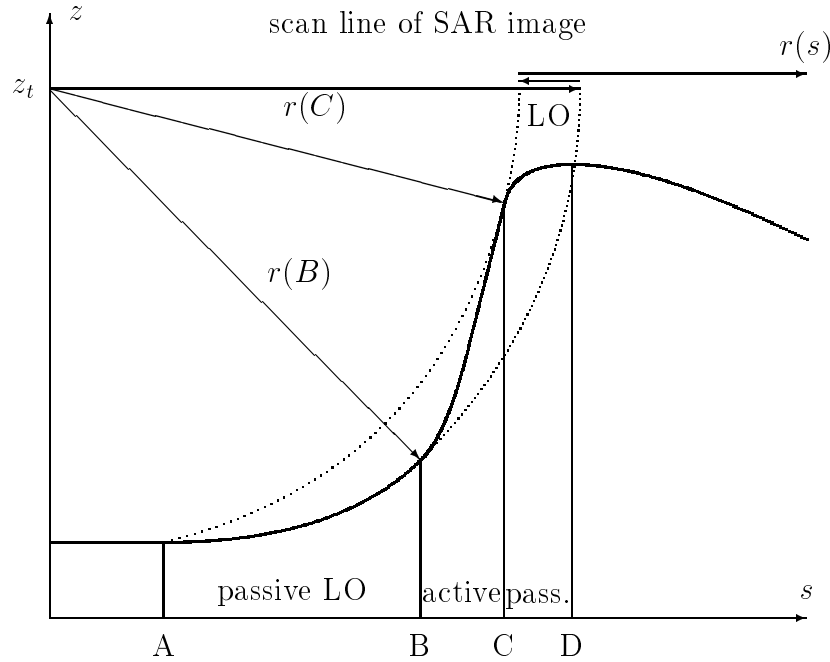


Figure 3: The elevation-range diagram of a SAR layover (LO).

Since layover only occurs in an across track line (imaging time $t = const$) it necessitates to study profiles along iso-azimuth curves. At any time t , the (x, y, z) -DEM coordinate system can be transformed into a sensor ground-centered coordinate system (Fig. 3), where the sensor receives coordinates $(0, z_t)$ and any object point is located on a curve $(s, z(s))$. s measures the length of the ground projected iso-azimuth curve ($z = 0$) between the nadir point (x_t, y_t) ($s = 0$) and the object point (x, y) .

The relevant SAR mapping equation for the slant ranges $r(s)$ is defined by

$$r(s) = \sqrt{s^2 + (z_t - z(s))^2} \quad (1)$$

In the iso-azimuth curve $z(s)$ of a SAR image the phenomenon of layover occurs, when the range $r(s)$ decreases by increasing nadir distance s (Fig. 3). If a plane terrain (parallel to the x, y -plane) is mapped this function is continuously increasing since the height difference of the sensor and the imaged object point is constant ($(z_t - z(s)) = \text{const}$). In hilly or mountainous terrain the height $z(s)$ takes different values. This circumstance produces layover in the SAR image when the height $z(s)$ increases faster than the nadir distance s . This region is bounded by a local maximum $r(B)$ and a local minimum $r(C)$ in the range (i.e. $\frac{\partial r(s)}{\partial s} = 0$). It is called the active layover region. It can be calculated by differentiating

$$\frac{\partial r(s)}{\partial s} = \frac{s - (z_t - z(s)) \frac{\partial z(s)}{\partial s}}{r(s)} \quad (2)$$

Since $r(s) > 0$ for all $s > 0$, a decision function $R(s) = r(s) \frac{\partial r(s)}{\partial s}$ can be determined which decides for a given object point $(s, z(s))$ whether it belongs to an active layover region or not:

$$R(s) = s - (z_t - z(s)) \frac{\partial z(s)}{\partial s} \quad (3)$$

$R(s) \leq 0$ defines the active layover subregions. $R(s) = 0$ defines the exact boundaries $s = B$ and $s = C$ of the active layover region.

Since layover occurs, when more than one object point is mapped into a single image point, regions $s < B$ and $C < s$ are also part of the layover. Knowing the maximum range $r(B)$ and minimum range $r(C)$ of a layover interval, the ranges of passive regions $[A, B]$ and $[C, D]$ have to be within this range interval too.

Figure 4 shows the layover regions that have been extracted from the DEM data. The area corresponds to the windows in Figures 1 and 2.

3.2 SAR shadow in the DEM

Shadow in a SAR image is called the region, where an object point is not reached by any radar beam. Such object points produce a 'zero' signal in the image. Therefore shadow regions appear in the SAR image as dark areas corrupted by noise.

Among object points which are part of the shadow region we distinguish points belonging to the **active** (own shadow) region of an object or belonging to the **passive** (cast-shadow) region, which is produced by another object located closer to the sensor (Fig. 5). In the image space there is no such distinction.

Since shadow only occurs in an across track line (time $t = \text{const}$) it also necessitates to study iso-azimuth curves. The relevant SAR mapping equation for the look angle $\alpha(s)$ is defined by

$$\alpha(s) = \arctan \left(\frac{s}{z_t - z(s)} \right) \quad (4)$$

Figure 4: Layover from DEM

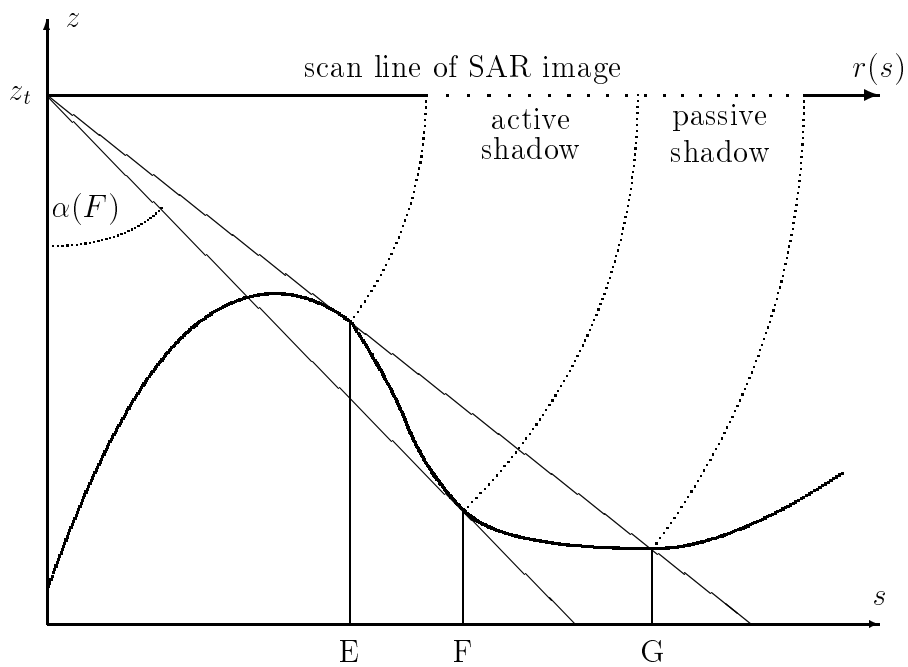


Figure 5: The elevation-range diagram of a SAR shadow

In the iso-azimuth line of a SAR image the phenomenon of shadow occurs, when the look angle $\alpha(s)$ decreases by increasing nadir distance s (Fig. 5). If a plane terrain (parallel to the x,y-plane) is mapped, this function is increasing when the height difference of the sensor and the imaged object point is constant. In hilly and mountainous terrain, shadows appear in the SAR image wherever the height $z(s)$ decreases faster than the nadir distance s increases. This region is bounded by a local maximum $\alpha(E)$ and a local minimum $\alpha(F)$ (i.e. $\frac{\partial\alpha(s)}{\partial s} = 0$), and is called active shadow region. It can be calculated by considering the sign of the derivative

$$\frac{\partial\alpha(s)}{\partial s} = \frac{z_t - z(s) + s\frac{\partial z(s)}{\partial s}}{r^2(s)} \quad (5)$$

A simple decision function $A(\alpha)$ can be defined similar to $R(s)$, to decide whether a given object point $(s, z(s))$ belongs to an active shadow region or not.

$$A(s) = z_t - z(s) + s\frac{\partial z(s)}{\partial s} \quad (6)$$

$A(s) \leq 0$ defines the active shadow parts. $A(s) = 0$ defines the exact boundaries $s = E$ and $s = F$ of the active shadow region.

In contrast to layover where two passive regions occurred here we have only one additional passive shadow region. It is located at the end of the active shadow, where the nadir distances s are increasing.

Both layover and shadow regions may also overlap. Two or more overlapping layover regions cause the multiplicity of the signals to further increase. Overlapping shadows result in the union of the single shadow regions in a mixture of active and passive parts. A shadow in a layover effects the multiplicity of the signal. All possible interactions between layover and shadow can be found in Strobl (1989) and Kropatsch and Strobl (1990).

3.3 Layover and Shadow Map

The discrete implementation of the above decision functions marks each cell of the DEM with labels layover, shadow or none, with further distinction between active and passive parts (Fig. 9 codes active layovers in white and passive parts in gray). Subsequent connected component labeling of this 'Layover and Shadow Map' (LSM) delivers the lists of regions corresponding to the regions in the SAR image.

We now summarize the algorithmic steps to calculate the LSM. The complete derivation is given in Kropatsch and Strobl (1990).

Let the DEM grid be defined by (i, j) with $i = 1, \dots, n; j = 1, \dots, m$; let the position of a grid cell be $(x_{i,j}, y_{i,j})$ with height $z_{i,j}$. The parameters of the flight path $(x_t(t), y_t(t), z_t(t))$ allow to compute the imaging time $t_{i,j}$ for every grid location by trilinear interpolation (Raggam 1988). The nadir distance $s_{i,j}$ can be calculated by

$$s_{i,j} = \sqrt{(x_t(t_{i,j}) - x_{i,j})^2 + (y_t(t_{i,j}) - y_{i,j})^2} \quad (7)$$

Using the spacing of the DEM grid $(\Delta x, \Delta y)$, the iso-azimuth direction $\phi_{i,j}$ can be approximated by central difference of the first derivative of imaging times

$$\cos \phi_{i,j} = \frac{t_{i+1,j} - t_{i-1,j}}{2\Delta x} \quad , \quad \sin \phi_{i,j} = \frac{t_{i,j+1} - t_{i,j-1}}{2\Delta y} \quad (8)$$

$$(9)$$

Using central differences again, the terrain slope in across track direction becomes

$$\frac{\partial z_{i,j}}{\partial s} = \frac{z_{i+1,j} - z_{i-1,j}}{2\Delta x} \cos \phi_{i,j} + \frac{z_{i,j+1} - z_{i,j-1}}{2\Delta y} \sin \phi_{i,j}. \quad (10)$$

The above computations deliver the values $s_{i,j}$, $z_t(t_{i,j})$, and $\frac{\partial z_{i,j}}{\partial s}$ to compute the decision functions $R(s_{i,j})$ and $A(s_{i,j})$ for the active parts of layover and shadow respectively.

If the passive parts are needed, the precise boundary ranges, $r(B)$ and $r(C)$, $r(E)$ and $r(F)$ resp., must be interpolated for every range profile that crosses such regions. A search across track must be performed in order to delineate the boundaries of the passive parts.

4 Matching

The comparison and matching of the two sets of regions (i.e. three layover regions in Figures 6 and 7) includes the following measurements:

- For a single region:
 - type: layover or shadow;
 - the center (of gravity);
 - the size and orientation;
 - shape characteristics like
 - * medial axis or
 - * segments of the boundary.
- For a local configuration of regions:
 - the distances between pairs of regions;
 - the relative positions between pairs of regions;
 - the adjacencies.
- For the entier image:
 - the parameters of the geometric mapping;
 - the accuracy of the resulting transformation.

Figure 6: 3 SAR-layover regions

Figure 7: match 3 DEM-layover regions.

Base level (1): 512×512

Level 5: 128×128

Figure 8: Levels 1 and 5 of layover curve pyramid

An experiment using a $2 \times 2/2$ curve pyramid demonstrates a coarse-to-fine strategy for efficient layover matching (Fermüller and Kropatsch, 1989 and 1990).

In a curve pyramid, the boundaries of all layover (or shadow) regions are stepwise reduced in resolution. Such curve reduction (Kropatsch, 1985) preserves the connectivity but shrinks the length of the curve (Kropatsch, 1987). In the bottom-up building process closed boundaries survive until a resolution cell completely covers the corresponding region. We therefore continue reducing the resolution until only a few boundaries of large layover regions remain. Fig. 8 shows the base level (1) of a curve pyramid derived from the SAR layover regions of Fig. 2 and level 5 of this pyramid. All major shape characteristics are preserved while a lot of small detail, which is mostly due to noise, disappeared.

Building this curve pyramid for both the SAR- and the DEM-regions reduces the complexity of a rough matching to a couple of large regions that have to be compared with each other. The accuracy of that match is then stepwise refined in a top-down process, that uses the match approximation of the level above to match the higher resolution curves. If implemented on parallel hardware this automatic control point determination algorithm would require only $\mathcal{O}(\log n)$ computational steps.

5 Possible extensions and drawbacks of the method

There are several possible extensions to the proposed method. We just enumerate a few of them without investigating the details.

- The calculation of the shadow regions in the DEM could also be interesting for other types of images, e.g. optical images with shallow sun angle.
- Using smoothness constraints and backscattering characteristics from the surrounding of layover regions, the integral information in (small) layover regions could be separated into its constituent parts in the ground reference.
- The proposed method depends on the knowledge of the sensor's flight path for the calculation of both the layover and the shadow regions. To relax this requirement, the DEM could be preprocessed to preselect the potential shadow and layover points by only rough estimations of the flight altitude and flight direction. A variation of this preselection was useful in the acceleration of the sequential implementation of the algorithm.
- The weakest (computational) component of the algorithm is the (sequential) search for the boundaries of the passive regions. Although the search in parallel across track curves could be done in parallel it still depends on the diameter of the region.

6 Conclusion

Figure 9: Layover and shadow map and geocoded SAR-image.

A feature-based approach to the integration of SAR-images and DEM data is presented. The features **layover** and **shadow**, which are characteristic for SAR images, are recognized independently in both data sets using properties of these features that are specific for the respective data set. Properties and relations of the resulting sets of layover and

shadow regions allow to match both data sets. A curve pyramid of the region shapes is an example for an efficient coarse-to-fine strategy for matching. The resulting geometric correspondences allow the SAR image to be transformed into the (map-) geometry of the DEM ('geocoding', Fig. 9), or, they allow to measure properties of other (local) features directly in the SAR image, thus avoiding consequences of resampling errors, and relating these measurements to the corresponding location in the DEM.

7 References

- [1] G. Domik. "Verfahrensentwicklung zur Analyse von digitalen Seitsicht-Radarbildern gebirgigen Geländes mittels digitaler Höhenmodelle und Bildsimulation." Ph.D. thesis, Tech. Univ. of Graz, Graz, Austria, Apr. 1985. Forschungsgesellschaft Joanneum, Graz, Austria, DIBAG Rep. 21.
- [2] C. Fermüller and W. G. Kropatsch. "Hierarchische Kontur-Beschreibung durch Krümmung." In A. Pinz, editor, *Wissensbasierte Mustererkennung*, pages 171–187, OCG-Schriftenreihe, Österr. Arbeitsgemeinschaft für Mustererkennung, R. Oldenburg, 1989. Band 49.
- [3] C. Fermüller and W. G. Kropatsch. "Multi-resolution shape description by corners." *Submitted to IEEE Transactions on Pattern Analysis and Machine Intelligence*, 1990.
- [4] B. Guindon. "Methods for automated control point acquisition in SAR images," in Proc. Intl. Workshop on SAR Image Rectification Techniques." Jan.14-16. 1987, pp. 29-32. Forschungsgesellschaft Joanneum, Graz, Austria, DIBAG Rep. 29.
- [5] W. G. Kropatsch. "*Hierarchical Curve Representation in a New Pyramid Scheme.*" Technical Report TR-1522, University of Maryland, Computer Science Center, June 1985.
- [6] W. G. Kropatsch. "Curve Representations in Multiple Resolutions." *Pattern Recognition Letters*, Vol. 6(No. 3):pp.179–184, August 1987.
- [7] W. G. Kropatsch and D. Strobl. "The Generation of SAR Layover and Shadow Maps From Digital Elevation Models." *IEEE Transactions on Geoscience and Remote Sensing*, Vol. 28, No. 1, pp.98–107, January 1990.
- [8] R. Kwok, J. c. Curlander, and S. S. Pang. "Rectification of terrain induced distortions in radar imagery," *Photogramm. Eng.*, vol. 53, pp. 507-513. May 1987.
- [9] E. Meier and D. Nüesch. "Geometrische Entzerrung von Bildern orbitgestützter SAR-systeme." *Bildmessung und Luftbildwesen*, vol. 54, no. 5, pp. 205-216, 1986.
- [10] M. Plößnig, B. Billington, and W. G. Kropatsch. "SHERLOCK - an intelligent system to locate control points in SAR" images and DEM. In *Proc. of the 2nd intl.*

Geosar-Workshop on 'Image Rectification for Spaceborne Synthetic Aperture Radar - Geocoded and Value-Added Products', Loipersdorf, Austria, January 1989.

- [11] M. Plößnig, W. G. Kropatsch, and D. Strobl. "SHERLOCK Supports the Geocoding of SAR Images." In *IGARSS'89: Quantitative Remote Sensing: An Economic Tool for the Nineties*, pages 856–859, Vancouver, Canada, July 10-14 1989. Book 2.
- [12] J. Raggam. "An efficient object space algorithm for spaceborne SAR image geocoding." in Proc. ISPRS Comm. II Symp. (Kyoto, Japan), July 1988, vol. 2, pp. 393-400.
- [13] J. Raggam, D. Strobl, and G. Triebnig. "The rectification of SAR image data using a digital elevation model and image simulation techniques. Phase-B study for ERS-1 processing and archiving facility," Forschungsgesellschaft Joanneum, Graz, Austria, ESA Contract Rep. 6292/85/HGE-I, Tech. Note 17, Aug. 1986.
- [14] V. Sasse. "Correlation of SAR data with optical data and with simulated data," in Proc. Intl. GEOSAR Workshop on Geocoded and Value-Added Products. Forschungsgesellschaft Joanneum, Graz, Austria, DIBAG Rep. 40, Jan. 1989.
- [15] D. Strobl. "The effects of control point location errors on SAR geocoding in mountainous terrain," Diploma thesis, Technical Univ. of Graz, Austria, Jan. 1989. Forschungsgesellschaft Joanneum, Graz, Austria, DIBAG Rep. 37.
- [16] D. Strobl. "Paßpunktbestimmung in Radarbildern," in *Mustererkennung 1986*, ÖCG-Schriftenreihe der Österreichischen Arbeitsgemeinschaft für Mustererkennung, vol. 36, pp. 206-235, 1986.

æ